Hindawi
Science and Technology of Nuclear Installations
Volume 2023, Article ID 2536474, 23 pages
https://doi.org/10.1155/2023/2536474

Research Article

Shaking Table Testing of a Scaled Nuclear Power Plant Structure with Base Isolation

Linlin Song,[1,2] **Xueming Zhang**,[1,2] **Mingyang Wei**,[1,2] **Yunlun Sun**,[3] **Shicai Chen**,[4] **and Yan Chen**[3]

[1]*Ministry of Education Key Laboratory of Roads and Railway Engineering Safety Control, Shijiazhuang Tiedao University, Shijiazhuang 050043, China*
[2]*State Key Laboratory of Mechanical Behavior and System Safety of Traffic Engineering Structures, Shijiazhuang Tiedao University, Shijiazhuang 050043, China*
[3]*Chinergy Co., Ltd., Beijing 100193, China*
[4]*Beijing Key Laboratory of Earthquake Engineering and Structural Retrofit, Beijing University of Technology, Beijing, China*

Correspondence should be addressed to Xueming Zhang; zxmsll@126.com

Received 20 March 2022; Revised 13 May 2023; Accepted 9 October 2023; Published 31 October 2023

Academic Editor: Doddy Kastanya

To investigate the seismic performance and isolation effect of a high-temperature gas-cooled reactor, a 1/20 scale model including a reactor, a spent-fuel plant, and a nuclear auxiliary plant was fabricated. In addition, 220 mm lead-rubber bearings were designed and produced for use in the shaking table test, which included both isolated and nonisolated conditions. Two historical earthquake records and three artificial earthquake motions were used to input the ground motion in the tests. The results demonstrated that the seismic performance of the plant was better and that the structure was in an elastic state, under a safe shutdown earthquake event. Isolation bearings were found to effectively reduce the dominate frequency of the structure. The acceleration amplification factor of the superstructure was found to be less than 1. The isolation test results showed that the peak of the floor response spectrum at the pressure vessel support was less than 0.1 g. In the nonisolation test, the peak of the floor response spectrum was greater than 1 g. In the isolation test, the relative displacement of the structure was less than 1.1 mm, which was relatively small. The structure maintained a good isolation performance and exhibited improved safety under extreme ground motion.

1. Introduction

Seismic performance of a nuclear power plant (NPP) under extreme earthquakes is particularly important. The nuclear power plant system is complicated and requires high seismic resistance. After applying isolation, the standardized design can be achieved during the seismic design of a nuclear power plant [1]. Base isolation techniques are innovative strategies to protect structures from seismic and dynamic loadings [2]. Low-damping rubber (LDR) and lead-rubber (LR) seismic isolation bearings have been proposed for use in safety-related nuclear structures in the United States to mitigate the effects of severe horizontal earthquake shaking. They consist of multiple rubber layers in which the top and bottom surfaces are bonded to steel plates to restrict compressive deformation [3]. However, the engineering practice of isolation technology in NPP is subject to many limitations, such as the aging of rubber bearings [4]. A few large light water reactors were base-isolated in France (Cruas) and South Africa (Koeberg) in the 1980s. Some engineering measures can significantly improve the seismic design standards, and enhance the seismic resistance, of the overall structures of nuclear power plants that have adapted isolation technology.

In recent year, seismic isolation has been investigated on the use of isolation technology in NPP to reduce seismic demands on structures, systems, and components. The U.S. Department of Energy funded a series of studies related to the isolation of advanced reactors. Whittaker et al. [5] discussed the application of isolation technology to NPPs in

the United States. Yu et al. [6] used numerical simulation methods to research nuclear facilities on sites located in moderate and high seismic hazard areas, and the results indicated that the isolation system can effectively reduce the seismic risk and capital cost of NPPs. Parsi et al. [7] discussed the pathway of seismic isolation to standardized advanced nuclear reactors.

The Multidisciplinary Center for Earthquake Engineering Research (MCEER) team in the United States has conducted systematic research on nuclear power isolation systems. For example, Huang et al. [8–10] adopted a numerical simulation method to carry out a nonlinear dynamic analysis and evaluate the seismic safety of a base-isolated nuclear power plant and its important internal equipment, and the results were published in Chapter 12 of the ASCE 4–16 standards [11]. The Nuclear Regulatory Commission (NRC) of the United States has also conducted extensive research on the application of isolation technology in nuclear power plants, such as the study of a mechanical model of rubber bearings under ultimate loads [12] and the probabilistic risk analysis of nuclear facilities under base isolation [13], and the results of this research have been summarized in the ASCE 43 standards [14].

The Korea Atomic Energy Research Institute (KAERI) and the Korea Electric Power Corporation (KEPCO) funded a five-year research program on the isolation of nuclear power plants and obtained significant research results regarding the implementation measures and standards of isolation, the performance standards of pipeline structures, seismic vulnerability, and the risk assessment of isolated plants [15–18].

However, there has been little research on the base isolation of NPPs, especially considering both structure and equipment. It is obvious that base isolation can improve the seismic margin of the plant and equipment. Therefore, it is necessary to conduct shaking table tests to investigate the effects of base isolation. In this paper, a high-temperature gas-cooled reactor NPP model was made to the base-isolated and nonisolated shaking table tests. The seismic performances of the structures were analyzed, and the influences of base isolation on the dynamic response of the plant and its internal main equipment under both design and beyond-design ground motion were, respectively, investigated. The results were compared with those of experiments under nonisolated states to verify the effects of the isolators.

2. Shaking Table Test

2.1. Prototype Structure. China's Huaneng Shidaowan high-temperature gas-cooled reactor nuclear power plant is the first demonstration project in the world to successfully commercialize fourth-generation nuclear power technology and comprises a reactor plant, a nuclear auxiliary plant, and a spent-fuel plant. The structure is irregular in both horizontal and vertical arrangements. The plane is L-shaped; the reactor is located in the corner, and the spent-fuel plant and the nuclear auxiliary plant are located on either side of the reactor. The thickness of the reinforced concrete shear wall at the reactor and the auxiliary plant is 1000 mm, and the thickness of the shear wall at the spent-fuel plant is 1500 mm. The thickness of the reinforced concrete protecting tube at the pressure vessel is 2400 mm. The elevation of the foundation is −15.55 m and that at the top of the reactor plant is 44.10 m. The elevations at the top of the spent-fuel plant and the auxiliary plant are 36.08 m and 21.60 m, respectively. The structure of NPP is illustrated in Figure 1.

2.2. Design of the Test Specimen

2.2.1. NPP Model. The scale of the plant model was determined to be 1/20 by considering the payload and size of the shaking table. The model was constructed of particulate concrete material, and the mix proportion of cement, yellow sand, lime, and water was 1 : 0.5 : 0.6 : 1.88 [19]. The compressive strength of the concrete cube was 8.6 MPa. The density of the microconcrete was similar to that of the prototype concrete, so the similitude parameter of density was set as 1. The elastic modulus similitude parameter was set as 1/4, and the scales of each physical quantity are listed in Table 1.

To ensure the accuracy of the experiments, the specimen was as least simplified as possible. The models of the reactor plant and the spent-fuel plant were made according to the prototypes, and the openings of the floor and stairs were retained. The nuclear auxiliary plant model had a simplified wall according to equivalent stiffness, and its internal wall was simplified as two crossed walls, as illustrated in Figure 2.

The internal template was made of foam and had little effect on the strength of the structure; the internal structure of the test model was complicated with many openings and internal walls, and it was a closed structure, leading to the impossibility of dismantling the inner template. The method of layered construction was adopted for the concrete specimen; after the completion of each layer of construction and maintenance, the next layer of the template was created. The construction of the concrete model is illustrated in Figure 3.

2.2.2. Isolator. The raft foundation was used on the prototype nuclear power plant, and 329 lead-rubber bearings (LRBs) were designed for the isolation layer under the foundation. LRB1100, LRB900, and LRB800 were selected to effectively avoid structural torsion and meet the requirements of isolation. In the model test, the stiffness similarity ratio compared to the prototype was adopted to the isolator. Considering the fabrication of isolation bearing and the connection between the bearing and shaking table, four LRB220 were applied as the isolation bearing of the model. The basic parameters of the isolators are listed in Table 2, and the hysteresis curve of a single lead-rubber bearing is presented in Figure 4.

The isolators were placed under the foundation slab. The same model was tested with and without isolation bearings, it was necessary to consider the installation and removal of the isolators. Therefore, they were arranged at the corner of the foundation slab, as shown in Figure 5. To ensure that the isolators could be successfully installed and removed, round

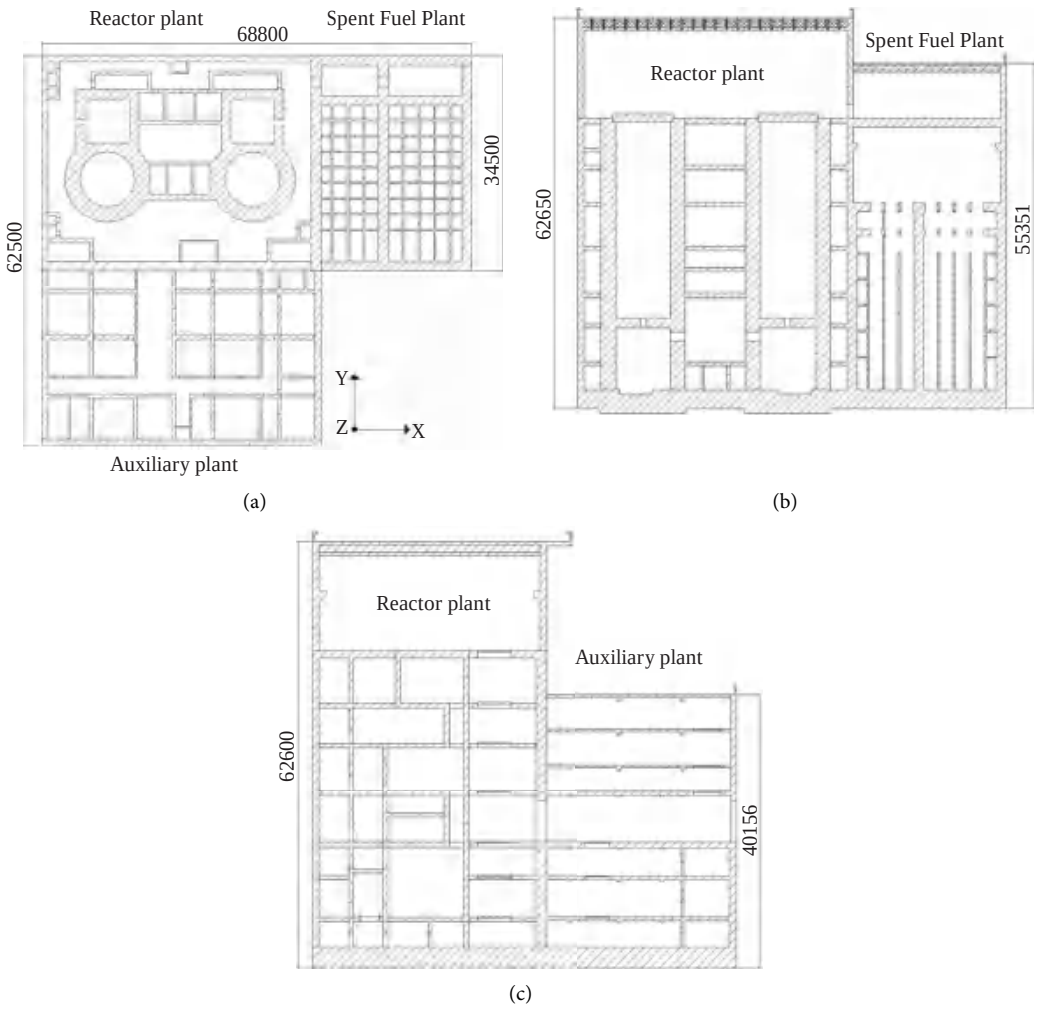

Figure 1: NPP layout. (a) Top view. (b) Elevation view of the reactor and spent-fuel direction. (c) Elevation view of the reactor and auxiliary direction.

Table 1: Similarity law of the NPP model.

Type	Physical quantity	Dimension	Similar coefficient
Geometry size	Size l	(L)	$S_l = 1/20$
Material properties	Elastic modulus E	(FL^{-2})	$S_E = 1/4$
	Density ρ	$(FL^{-4}T^2)$	$S_\rho = 1$
	Poisson's ratio μ	—	$S_\mu = 1$
	Strain ε	—	$S_\varepsilon = 1$
	Stress σ	(FL^{-2})	$S_\sigma = S_E\ S_\varepsilon = 1/4$
	Equivalent mass density ρ_e	$(FL^{-4}T^2)$	$S_{\rho e} = 1$
Dynamic indicators	Time T	(T)	$S_T = S_L\sqrt{S_{\rho_e}/S_E} = 0.1$
	Frequency ω	(T^{-1})	$S_\omega = 1/S_T = 10$
	Damping ratio ζ	—	$S_\zeta = 1$
	Acceleration amplitude a	(LT^{-2})	$S_a = S_E/(S_L\ S_{\rho\varepsilon}) = 5$
	Stiffness K	(FL^{-1})	$S_K = SE\ S_l = 0.0125$
	Mass m	$(FL^{-1}T^2)$	$S_m = S_{\rho\varepsilon}\ S^3{}_l = 1.25E-4$

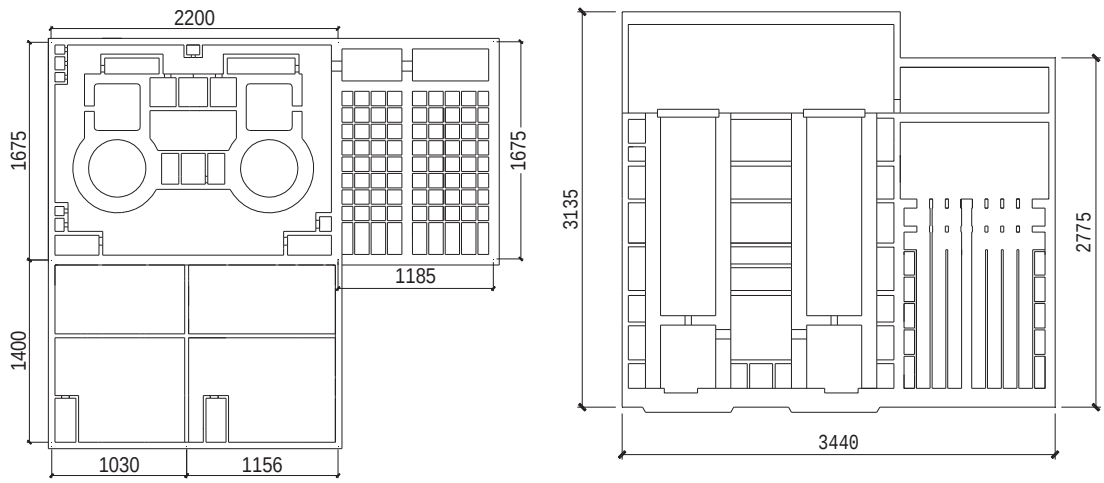

(a) (b)

Figure 2: Design drawing of the concrete specimen. (a) Plane; (b) sectional view of the reactor and the spent-fuel plant.

(a) (b)

Figure 3: Construction of the concrete model. (a) Shear wall; (b) spent-fuel pool.

Table 2: Rubber bearing performance parameters.

Parameters	Unit	Value
Model	—	LRB220
Size	mm	220.00
Design displacement	mm	100.00
Average pressure	MPa	1.98
Total rubber thickness	mm	40.00
Yield force	kN	6.70
Vertical stiffness	kN/m	440
Vertical bearing capacity	kN	314
Horizontal performance value at 100%		
Equivalent stiffness	kN/m	475
Equivalent damping ratio	%	12.3
Horizontal performance value at 250%		
Equivalent stiffness	kN/m	345
Equivalent damping ratio	%	12.3

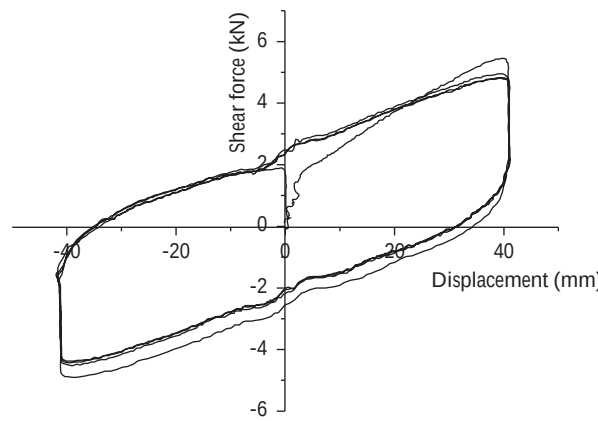

Figure 4: Hysteresis curves of lead-rubber bearing.

steel columns were placed under the isolators to increase clearance. The lower portions of the steel columns were connected to the shaking table by steel sheets, the upper portions were connected with the lower steel sheets of the isolators by bolts, and the upper steel sheets of the isolators were connected with the base plate of the specimen. The assembly of the isolators is illustrated in Figure 6.

To ensure the accurate positioning and installation of the isolators, the model was made on a simulation table with the same size as that of the shaking table, and the isolators were installed in advance. Reinforcements on the steel sheets of isolation bearings were implanted into the bottom plate of the model to fix both the model and isolation bearings. The on-site installation of the isolation bearings is depicted in Figure 7.

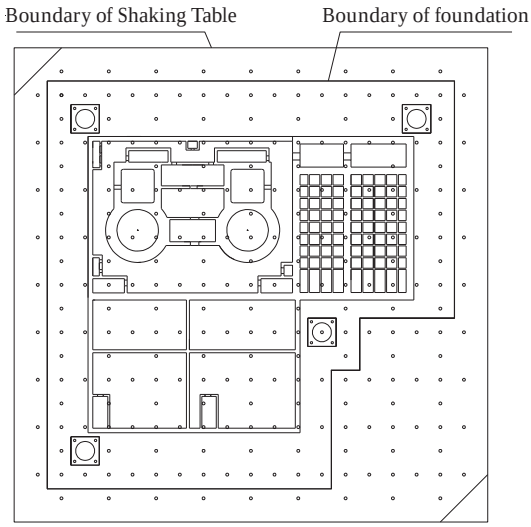

Figure 5: Layout of isolation bearing.

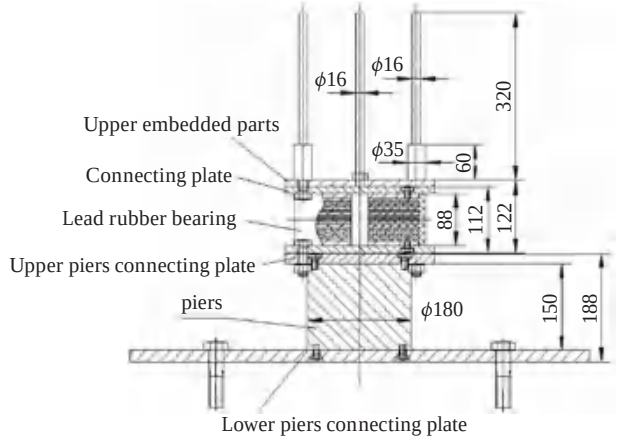

Figure 6: Assembly drawing.

(a) (b)

Figure 7: On-site installation of isolation bearings. (a) Isolation bearings and steel column; (b) reinforcement.

2.2.3. Equipment Models. The pressure vessel and the steam generator of the nuclear power plant were selected for investigation. The scale of the equipment model was 1/20, which was consistent with the scale of the NPP model. Wall thickness was determined by a stiffness similarity ratio. The outer diameter of the pressure vessel model was 299 mm with a thickness of 12.3 mm, and the outer diameter of the steam generator model was 194 mm with a thickness of 6.3 mm. The equipment installations of the pressure vessel and the steam generator are illustrated in Figure 8.

(a) (b)

Figure 8: Equipment installation. (a) Hoisting; (b) planting.

The method adopted to fix the equipment was the use of welded steel bars to simulate the lateral and vertical supports of the two pieces of equipment. One end of the steel bar was welded to the equipment, and the other end was embedded in the wall cylinder and floor of the pressure vessel and bound with the steel bars of the wall cylinder and floor. Finally, the concrete is poured outside the steel framework (see Figure 9).

2.3. Test Device. The experiments were conducted in three directions on a 5×5 m shaking table at the Institute of Engineering Mechanics, China Earthquake Administration. The specific parameters were as follows: a table size of 5×5 m, a maximum load of 30 t, a maximum overturning moment of 80 t·m, maximum strokes of ±500 mm along the x- and y-directions and ±200 mm along the z-direction, a maximum full-load acceleration of 2.0 g along the x- and y-directions, a no-load acceleration of 3.0 g, a maximum full-load acceleration of 2.0 g along the z-direction, a no-load acceleration of 2.0 g, maximum speeds of 1.5 m/s along the x- and y-directions and 1.2 m/s along the z-direction, and an operating frequency of 0.1–100 Hz.

The test specimen on the shaking table is depicted in Figure 10. Dynamic acquisition systems made by Jing Ming Technology Co., Ltd (Yangzhou, China) were adopted to collect the test data. The acquisition frequency of this test was set as 1000 Hz, and 64-channel acceleration and displacement signals and strain signals of 64 channels were collected synchronously (see Figure 11).

2.4. Measuring Point Arrangement. Three-component acceleration sensors (A1–A7) were used to measure the acceleration response of the structure, and Figure 12 illustrates the arrangement of the acceleration sensors. Sensor A1 was placed on the foundation floor, sensor A2 was placed at the vertical support of the pressure vessel, sensors A3–A5 were located at the floors of the key equipment, sensor A6 was

Figure 9: Equipment supports.

Figure 10: Test specimen.

positioned at the concrete roof of the top pressure vessel barrel, and sensor A7 was located on the top plate. Pull-on-the-rope displacement sensors were employed to measure the displacement of the isolators and each layer. Due to the closed structure of the nuclear power plant model, sensors A2–A10 were prearranged during the construction process. Regarding the two sensors not shown in Figure 12, sensor A11 was placed on the top of the spent-fuel plant and sensor A12 was placed on top of the auxiliary plant.

Pull-on-the-rope displacement sensors were respectively arranged along the x- and y-directions to measure the relative displacement of the isolators and the displacement of the test model. The x-direction displacement sensors were arranged at different elevations of the reactor plant and the

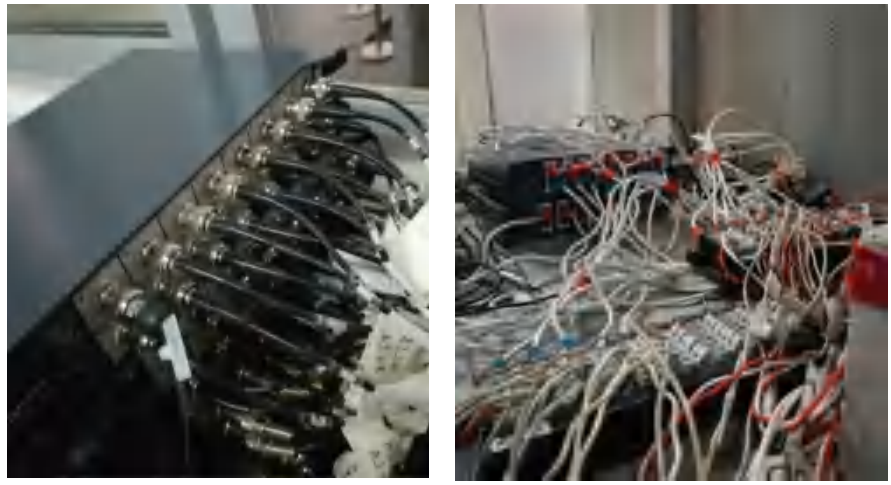

(a) (b)

Figure 11: Acquisition instrument. (a) Acceleration and displacement measurement; (b) strain measurement.

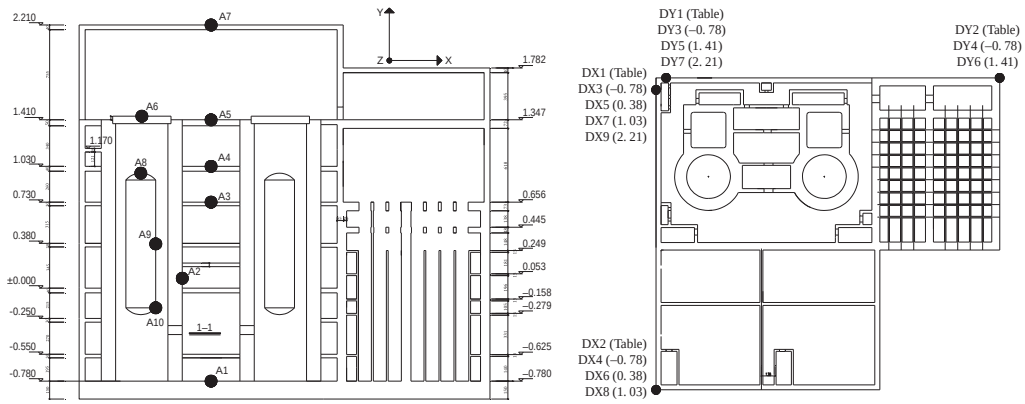

(a) (b)

Figure 12: Sensors arrangement. (a) Acceleration sensors; (b) pull-on-the-rope displacement sensors (the number was the model elevation).

(a) (b)

Figure 13: Sensor installation diagram. (a) Acceleration sensor of equipment outer wall; (b) strain gauges on wall.

auxiliary plant, and the *y*-direction displacement sensors were arranged at different elevations of the reactor plant and the spent-fuel plant.

According to the shape of the plant, the concrete at the junction of the reactor plant and the nuclear auxiliary plant was prone to damage. Therefore, six sets (three in each

group) of strain gauges were placed along the height of the easily damaged position with angles of 45° between each of the strain gauges. The installation of the sensors is presented in Figure 13.

2.5. Selection of Ground Motions. Three artificial earthquake motions and two historical earthquake records were used in the tests. The artificial earthquake motions were, respectively, generated by the uniform hazard spectrum (UHS), RG1.60, and SL-2 spectra. UHS was generated by a specific site condition [20]. The SL-2 spectrum called ultimate safety earthquake spectrum was obtained from the safety evaluation report of the nuclear power plant. The RG1.60 spectrum was obtained from Regulatory Guide1.60 [21]. To explore the influence of the uniform hazard spectrum (UHS) on the seismic and isolation performances of the structure, the historical records of Parkfield and San Fernando were selected according to the shape of UHS. The peak acceleration of the five motions was adjusted to be the same as that of the SL-2 spectrum, and the response spectrum curves are illustrated in Figure 14.

The test was carried out in two stages; the first was the isolation test, and the isolators were then removed for the nonisolation test. The two tests were both carried out with bidirectional and tridirectional ground motion. The peak value increased gradually from 0.85 g to 1.7 g. After each magnitude was complete, white noise was input for frequency sweeps. According to the similitude relationships of time, the ground motions were input by a scale of 0.1.

3. Test Results and Analysis

3.1. Acceleration Response. Figure 15 presents the acceleration amplification factor of the NPP model with the peak was 0.85 g. The amplification factor was about 0.1 and 0.2~0.4 at the base and top of the model, respectively. The results were less than the results of Tagliafierro et al. [22] and Zhu et al. [23], where amplification factors were about 0.3 and 0.5, respectively. It can be seen that the structure with isolators can reduce the acceleration response of the upper structure. The acceleration of the structure with isolators was more evenly distributed in the horizontal direction, and the difference between the motions was small. However, there was an obvious amplification effect on the top layer, and the amplification effect in the y-direction was greater than that in the x-direction, and this occurred because of the y-direction, as the weak-axis direction of the structure, making the dynamic response of the structure more evident. In the horizontal direction of the structure without isolators, the difference of the amplification effect among the motions was large. Along the x-direction, the amplification of UHS and RG1.60 was particularly obvious. This may be the main frequency content of the motions close to the natural frequency of the model. Along the y-direction, the amplification factor of RG1.60 was the greatest, and those of the two historical earthquake records were the smallest. Meanwhile, the amplification factor of UHS and SL-2 was placed in the middle.

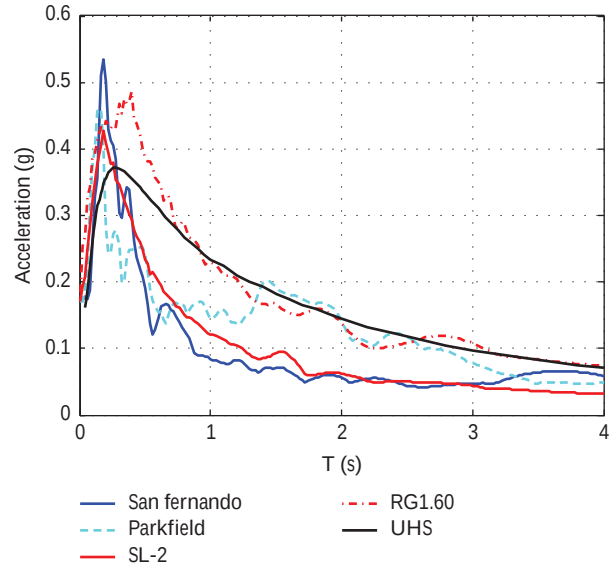

Figure 14: Response spectrums for testing.

In the vertical direction of the structure, the vibration of the foundation slab caused by the isolation layer was large, and the acceleration changed greatly in the vertical direction of the foundation plate. In the middle of the structure, acceleration was small, and the amplification on the top of the structure changed was relatively obvious. Due to the small differences between the vertical stiffness of the isolation layer and the NPP model, the horizontal isolators had less effect on the vertical isolation of the structure, and the amplification factor of each layer in the structure was greater than that of the table. For the structure without isolators, the acceleration amplification factor was greater, and the amplification effect of the top layer was more obvious.

Figure 16 presents the respective acceleration amplification factors of the structure with isolators with the peak accelerations were 1.28 g and 1.70 g. With an increase in the floor height, the acceleration amplification factor of the structure increased. Under a peak value of 1.28 g, the amplification factor in the upper layer structure was within 0.3 along the x-direction, which in the middle layers was between 0.1 and 0.3 along the y-direction. At the top of the structure, the amplification factor was 0.47. Under a peak value of 1.7 g, the maximum amplification factor of the structure along the x-direction was 0.43 and that along the y-direction was less than 0.25. Therefore, the isolated structure could still maintain a good isolation effect under overdesign ground motion.

Figure 17 presents the acceleration time-history curve and the corresponding Fourier spectra of the pressure vessel support (measuring point A2) under the isolated and nonisolated actions (the peak value was 0.85 g). In the isolated state, the peak acceleration in both directions was approximately 0.1 g, which was less than the input value. As can be observed in the spectrogram, the frequency distributions of UHS in the x- and y-directions were wide, and the distribution was uniform within 10 Hz. The SL-2 spectrum exhibited a peak in the y-direction, while the RG1.60

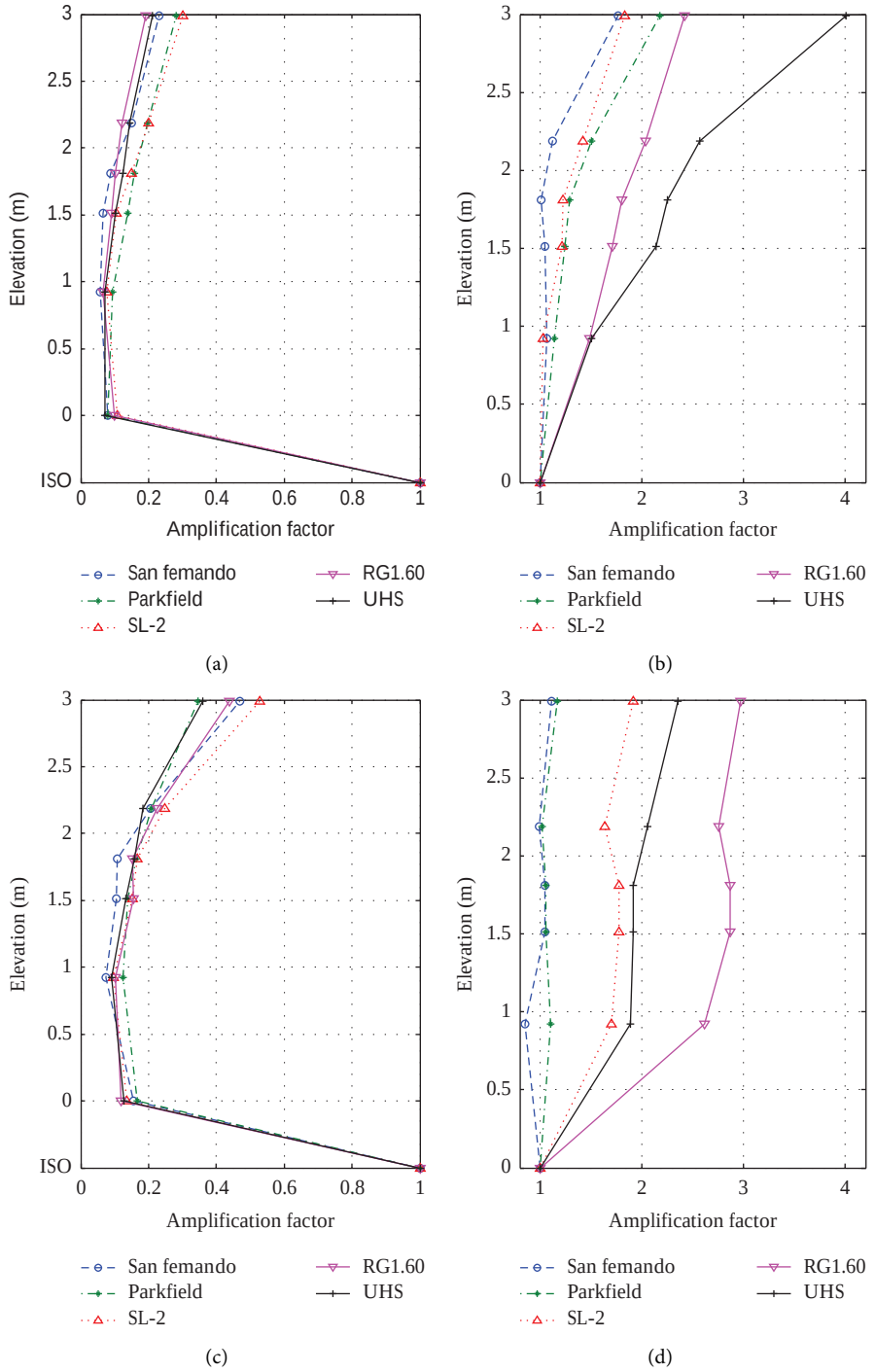

Figure 15: Continued.

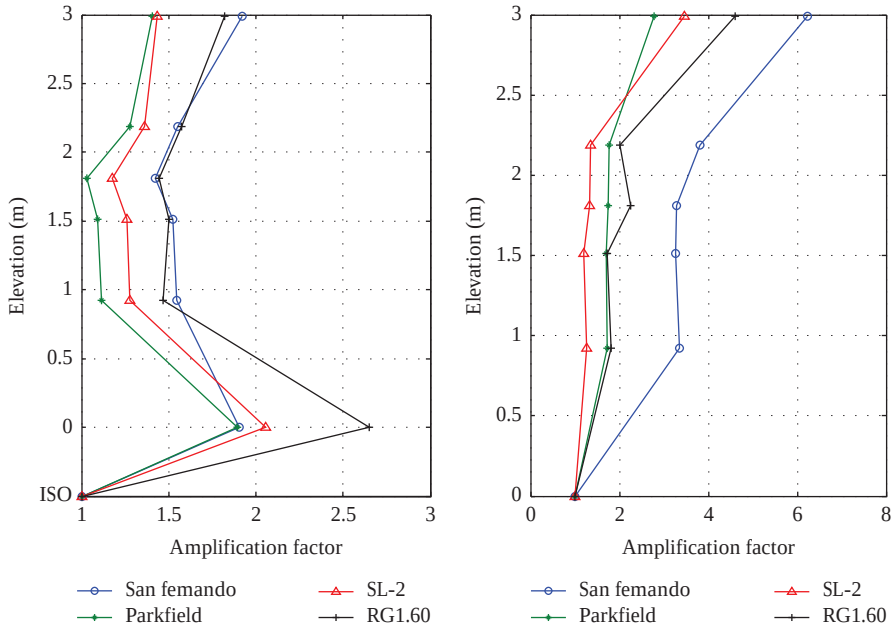

Figure 15: Acceleration amplification factor (0.85 g). (a) Structure with isolations along the *x*-direction; (b) structure without isolations along the *x*-direction; (c) structure with isolations along the *y*-direction; (d) structure without isolations along the *y*-direction; (e) structure with isolations along the *z*-direction; (f) structure without isolations along the *z*-direction.

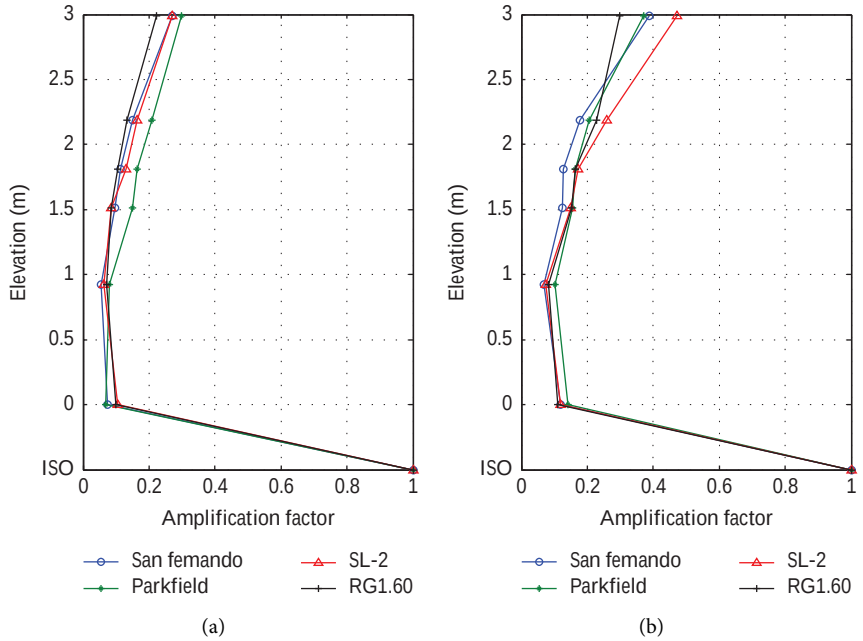

Figure 16: Continued.

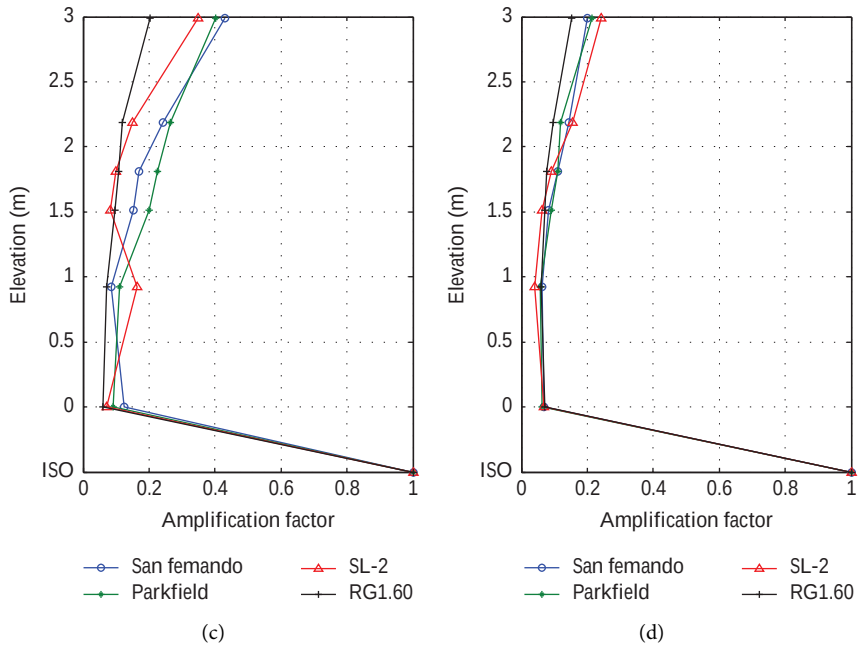

Figure 16: Acceleration amplification factor of isolation structure. (a) 1.28 g along the x-direction; (b) 1.28 g along the y-direction; (c) 1.70 g along the x-direction; (d) 1.70 g along the y-direction.

spectrum exhibited peaks in both the x- and y-directions. The distributed range of each spectrum in the y-direction was wider than that in the x-direction, which was related to the strong and weak axis of the structure. In the nonisolated test, the acceleration time history of the measurement point was greater than the input value, indicating that the acceleration at point A2 was amplified. Compared with the isolation tests, the nonisolated frequency had a relatively backward range, and the peak frequencies of the spectrogram under different motions had different ranges. This indicated that the responses of the structure to different motions were quite different.

To investigate the effects of the horizontal isolators on vertical motions, Figure 18 presents the acceleration response and corresponding Fourier spectrum of the pressure vessel support (measurement point A2) when the input peak value was 0.85 g. It can be concluded from the time history that, except for the San Fernando motion, the horizontal isolators had little effect on the peak acceleration of this point. Due to the existence of the isolators, the waveforms of the same ground motions were quite different from that in the nonisolated test, and the performance of the artificial ground motion was more obvious. In the nonisolated test, the vibration caused by ground motions SL-2 and RG1.60 basically stopped after 3 s, while the vibration of the measuring point in the isolated test stopped after 4 s. It is evident from the spectrogram that, in the isolated tests, the spectrum of the measuring point was concentrated at about 20 Hz, whereas in the nonisolated state, the frequency range of the measuring point was between 30 and 40 Hz. This indicates that the horizontal isolators had an impact on the vertical motion of the structure and that the vertical stiffness of the isolated layer was weaker than the overall stiffness of the structure.

Figure 19 presents the three-direction acceleration time-history curve at the middle part of the equipment (A9), and the isolation effect of the base isolation bearings on the equipment was obvious. Due to the impact of the isolators, the vibration time of the structure under isolation was longer, but the amplitude was very small, and the peak acceleration under all conditions was approximately 0.1 g. The horizontal frequency was concentrated around 10 Hz, and the vertical frequency was around 20 Hz. In the structure without isolators, the peak accelerations all exceeded 1 g, and the peak values of the artificial earthquake motions generated by the UHS and RG1.60 spectra were larger than those of others. The horizontal spectra were concentrated between 10 and 30 Hz, and the vertical spectra were mostly concentrated after 30 Hz. This implies that the vertical stiffness of the structure was large.

Figure 20 presents the acceleration amplification factor of measuring point A9 in the middle of the pressure vessel under the action of a seismic wave of 0.85 g. The seismic isolators greatly reduced the peak acceleration response of the equipment. When the structure was not equipped with isolators, the amplification coefficients of the acceleration in the two directions were quite different; the amplification coefficients of the San Fernando and SL-2 waves along the x-direction were 1.04 and 1.1, respectively, and therefore, the amplification effect along the x-direction was small. In contrast, the amplification coefficients of the acceleration of the two waves along the y-direction were 1.27 and 2.07,

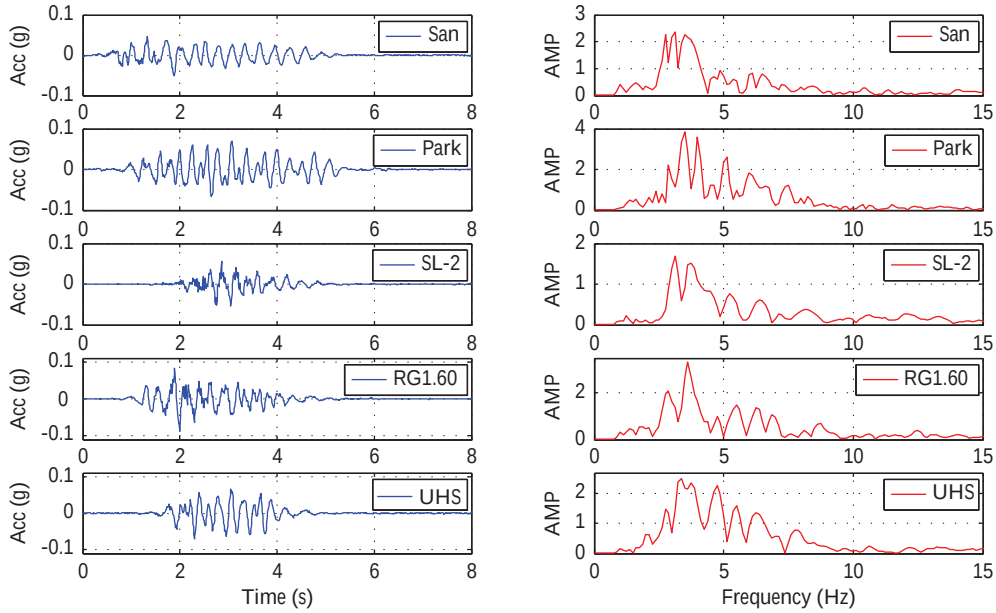

(a)

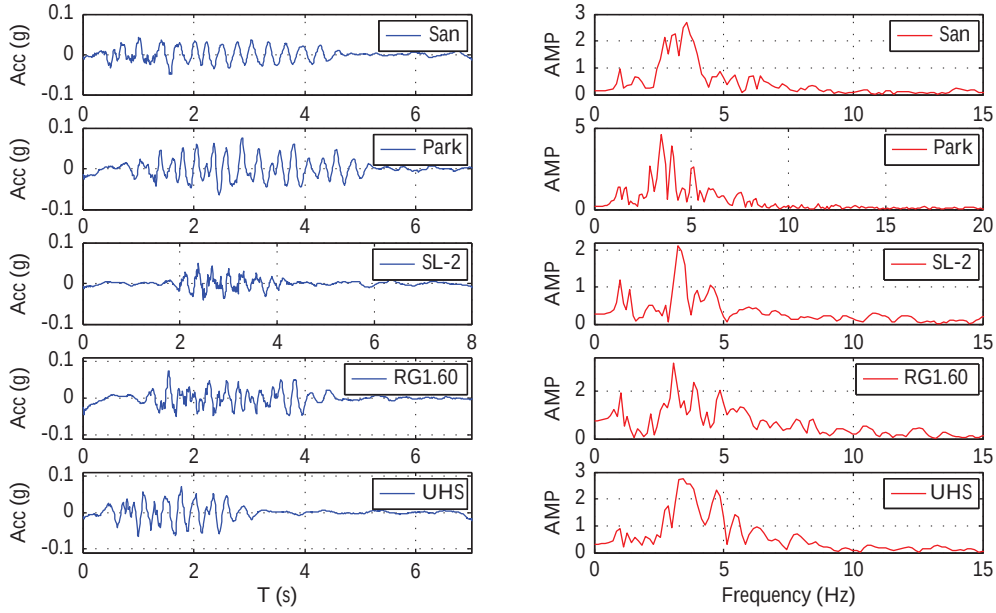

(b)

Figure 17: Continued.

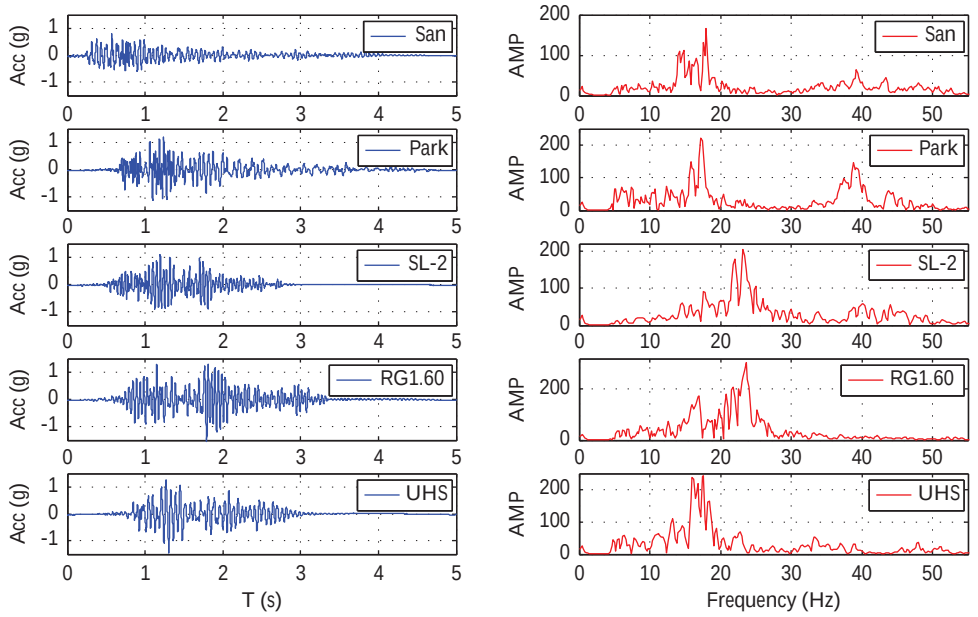

(c)

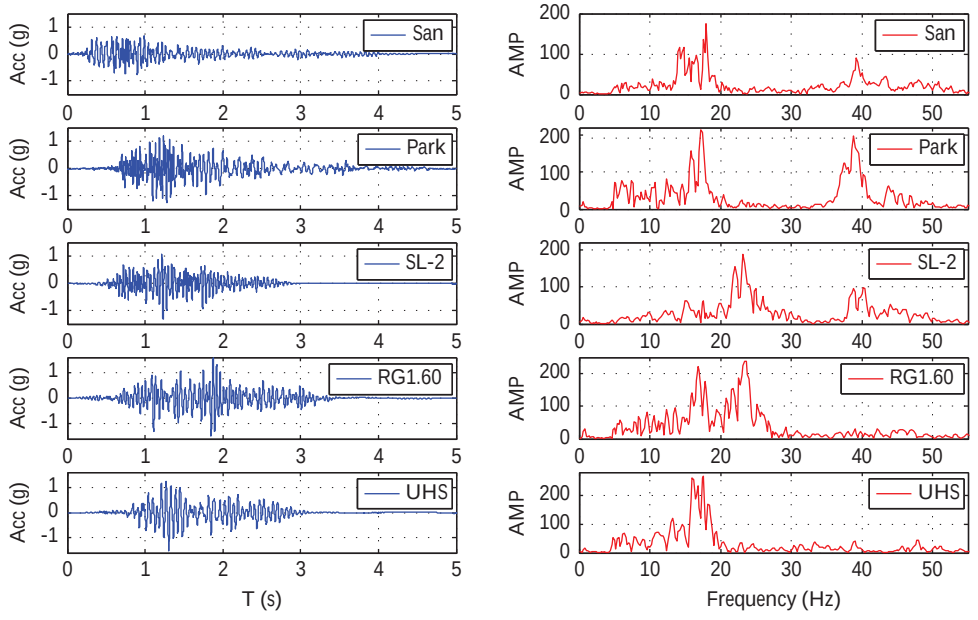

(d)

FIGURE 17: Horizontal acceleration response at pressure vessel support (A2). (a) Structure with isolations along the *x*-direction; (b) structure with isolations along the *y*-direction; (c) structure without isolations along the *x*-direction; (d) structure without isolations along the *y*-direction.

respectively, and therefore, the amplification effect was significant. The effect of the isolators on UHS was particularly obvious; the *x*-direction amplified coefficient of UHS was 1.89 in the nonisolated state and 0.13 in the isolated state.

3.2. Floor Response Spectrum. Due to the significance of the nuclear power equipment, the floor response spectrum at the equipment support is of importance. Therefore, the three-direction floor response spectrum was converted to the prototype according to the scale used for comparison in this

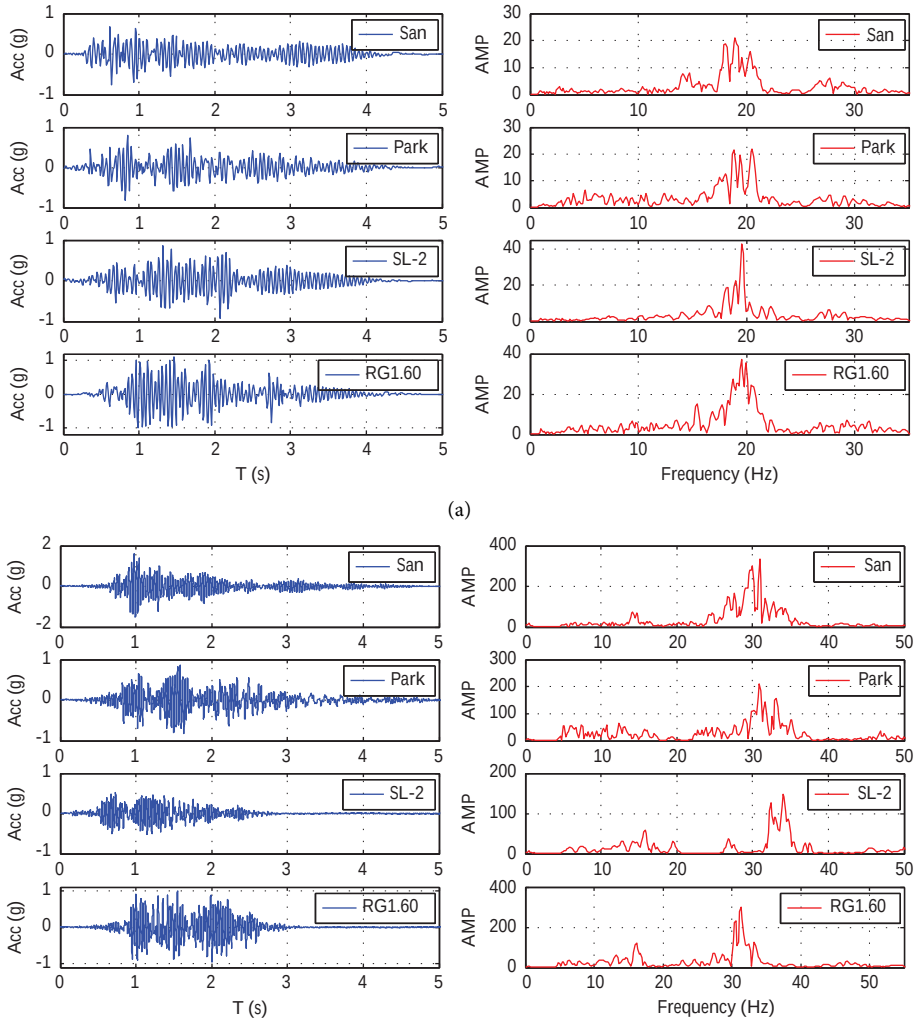

FIGURE 18: Vertical acceleration response at pressure vessel support (A2). (a) Structure with isolations along the z-direction; (b) structure without isolations along the z-direction.

work, and the results are presented in Figure 21. In the horizontal direction, the frequency of the response spectrum of the isolated floor was between 0.3 and 0.7 Hz, while that of the nonisolated floor was between 1 and 5 Hz; thus, the peak frequency of the floor response spectrum was effectively reduced by the isolators. The floor response spectrum of the structure with seismic isolators was primarily a single peak, the value of which did not exceed 0.1 g; in contrast, that of the structure without seismic isolators was primarily double peaks, and the peak values mostly exceeded 1 g. Therefore, horizontal isolation effectively reduced the peak value of the floor response spectrum. The amplitude of the seismic wave generated by UHS in the isolated state was higher over the entire range of frequencies. In the nonisolated state, the peak frequency of the artificial wave generated by UHS was lower and that of the Parkfield wave was higher. The frequency of the nuclear power equipment was primarily distributed after 7 Hz, which averted the peak of the floor response spectrum. However, the amplitude of the floor response spectrum resulting from the artificial earthquake motions generated by UHS and RG1.60 in this frequency band was relatively large and should be fully considered when the equipment is seismically resistant. Under the condition of horizontal isolation, the vertical floor response spectra of various working conditions exhibited large peaks at 2 Hz, while that in the nonisolated state was relatively flat without a prominent peak. Base isolators could therefore significantly reduce the horizontal floor response spectrum of a nuclear power plant, which is conducive to the seismic safety of the internal equipment of the plant and can increase the safety reserves of the structure and equipment. The adoption of base isolators can also greatly expand the site requirements of nuclear power plants.

3.3. Displacement Response. Figure 22 presents the maximum displacement of the upper floor of the structure under isolation relative to the shaking table under the action of a 0.85 g seismic wave. Under the action of different seismic waves, the main relative displacement of the model occurred in the isolated layer and that of each layer of the

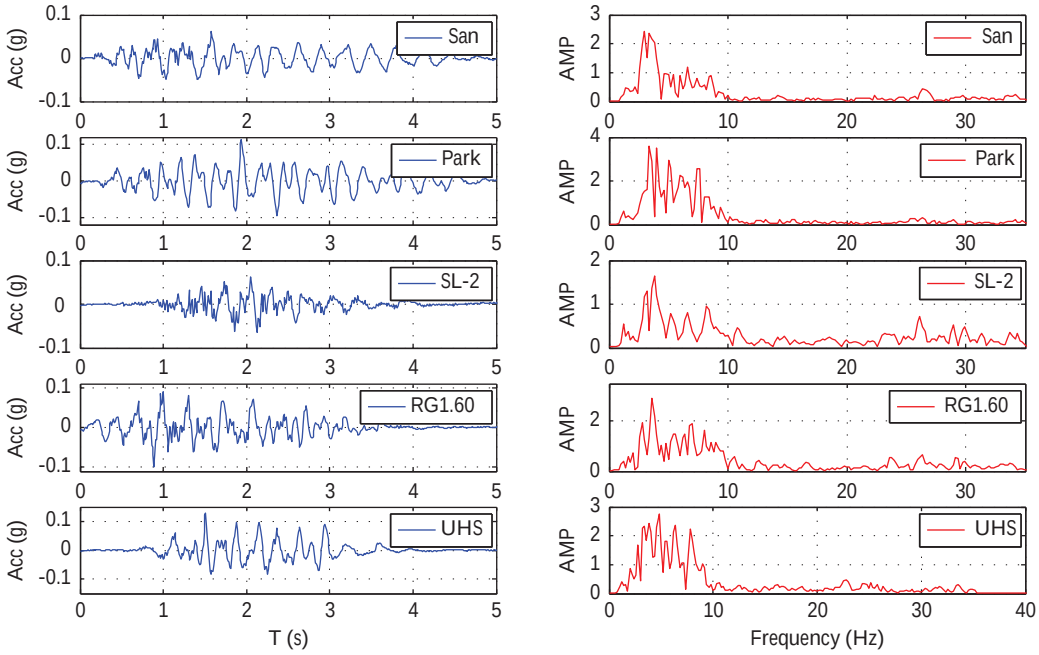

(a)

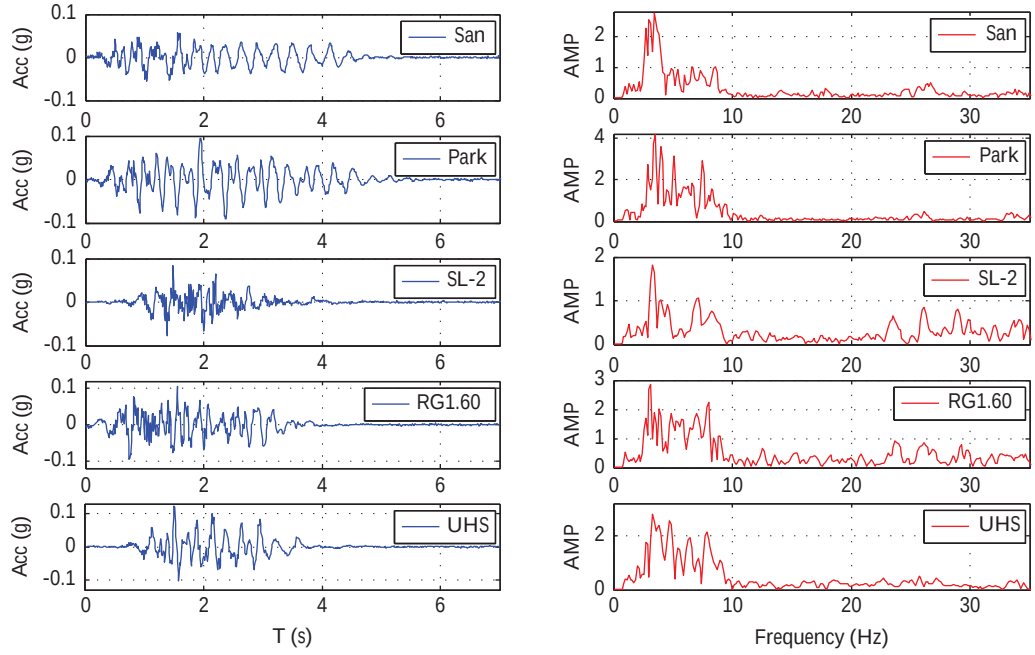

(b)

Figure 19: Continued.

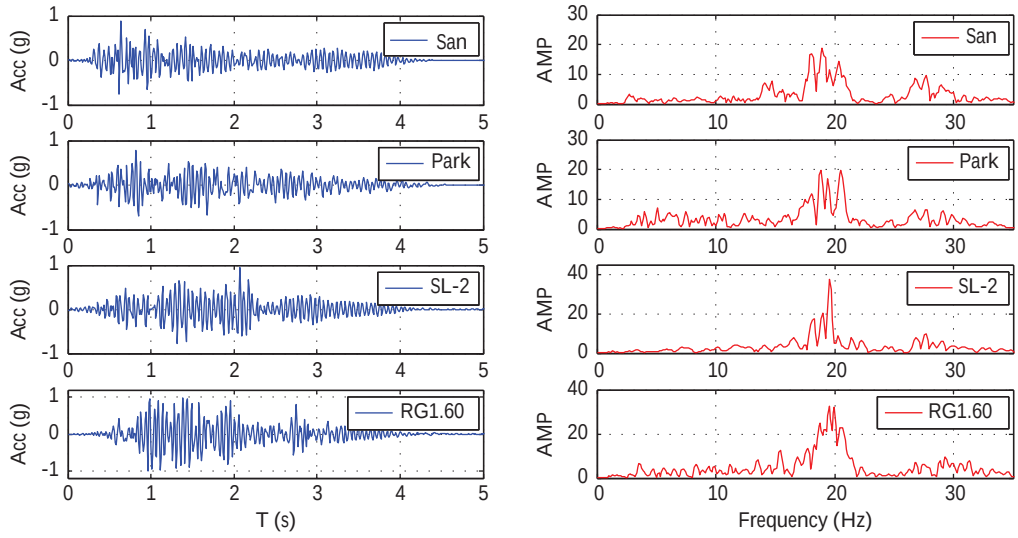

(c)

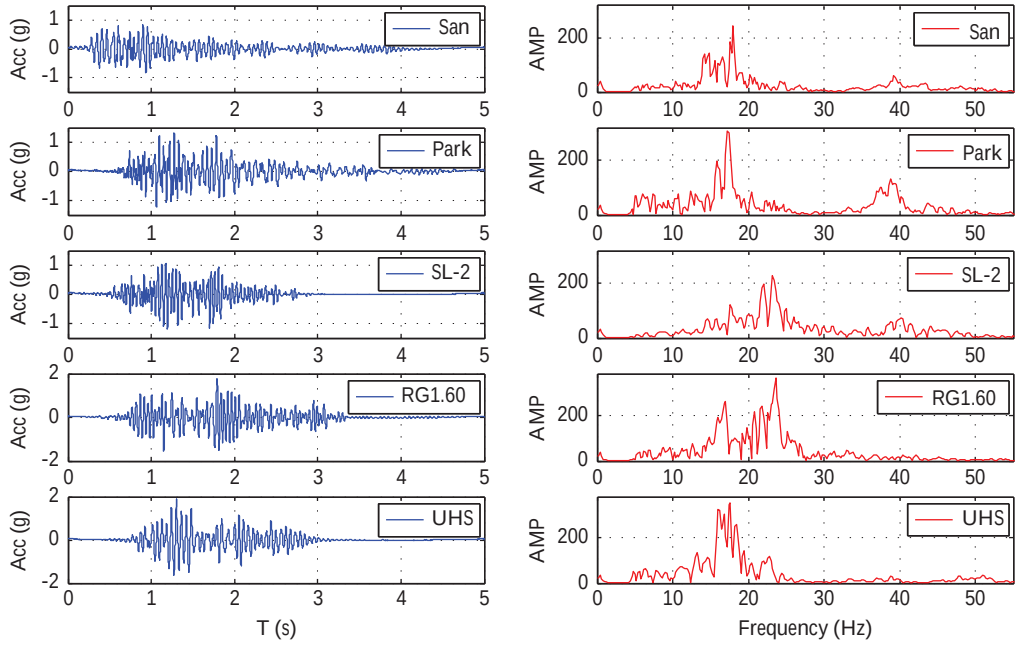

(d)

Figure 19: Continued.

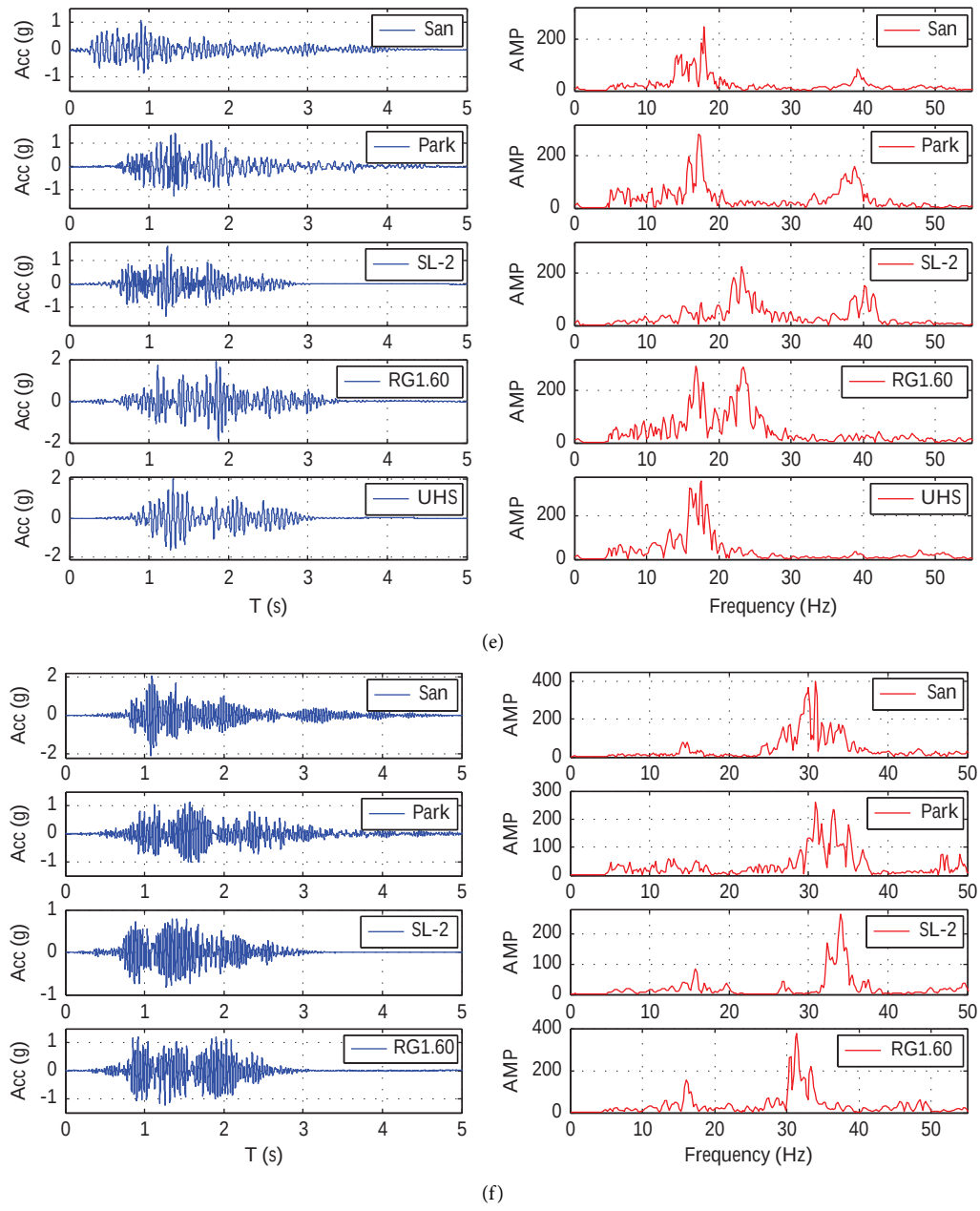

Figure 19: Response of acceleration in the middle of the pressure vessel (A9). (a) Structure with isolations along the x-direction; (b) structure with isolations along the y-direction; (c) structure with isolations along the z-direction; (d) structure without isolations along the x-direction; (e) structure without isolations along the y-direction; (f) structure without isolations along the z-direction.

superstructure was small. The relative displacement of the structure along the x-direction under the artificial wave generated by the RG1.60 spectrum had a maximum amplification factor of 5.07. Under the action of Parkfield and SL-2 waves, the relative displacements of the structure along the y-direction changed little. In contrast, the relative displacements of the middle part of the structure under San Fernando and RG1.60 waves were quite different, and the displacement at the top of the structure in the y-direction was increased, indicating that the amplification effect in the y-direction was greater than that in the x-direction.

The displacement time history of the reactor top relative to foundation under different seismic waves is presented in Figure 23. The displacement of the model structure in the isolated state was small. For the structure with isolators, the peaks of the displacement in the x- and y-directions generated by the UHS seismic wave were only 0.99 mm and 1.11 mm, respectively, whereas, in the nonisolated state, the peak values of displacement were 2.17 and 1.87 mm, which were, respectively, 2.19 and 1.68 times the values in the isolated state. This indicates that the isolators effectively limited the relative displacement between superstructures.

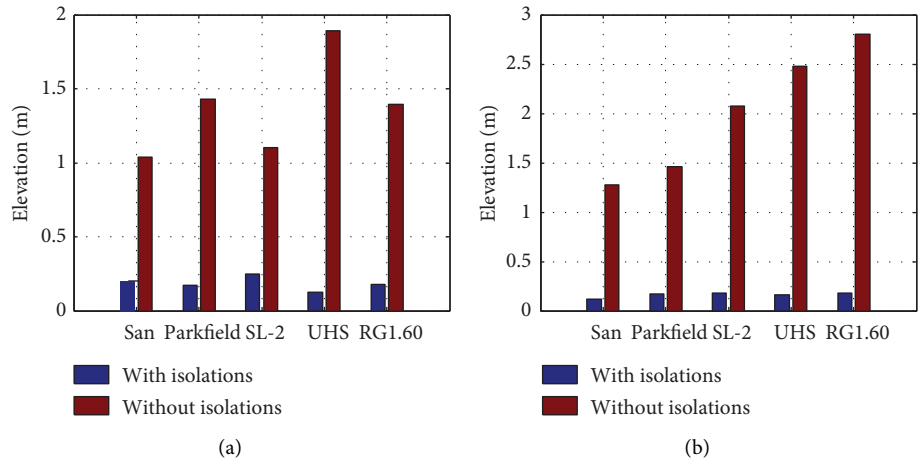

Figure 20: Acceleration amplification factor in the middle part of the pressure vessel (A9). (a) x-direction; (b) y-direction.

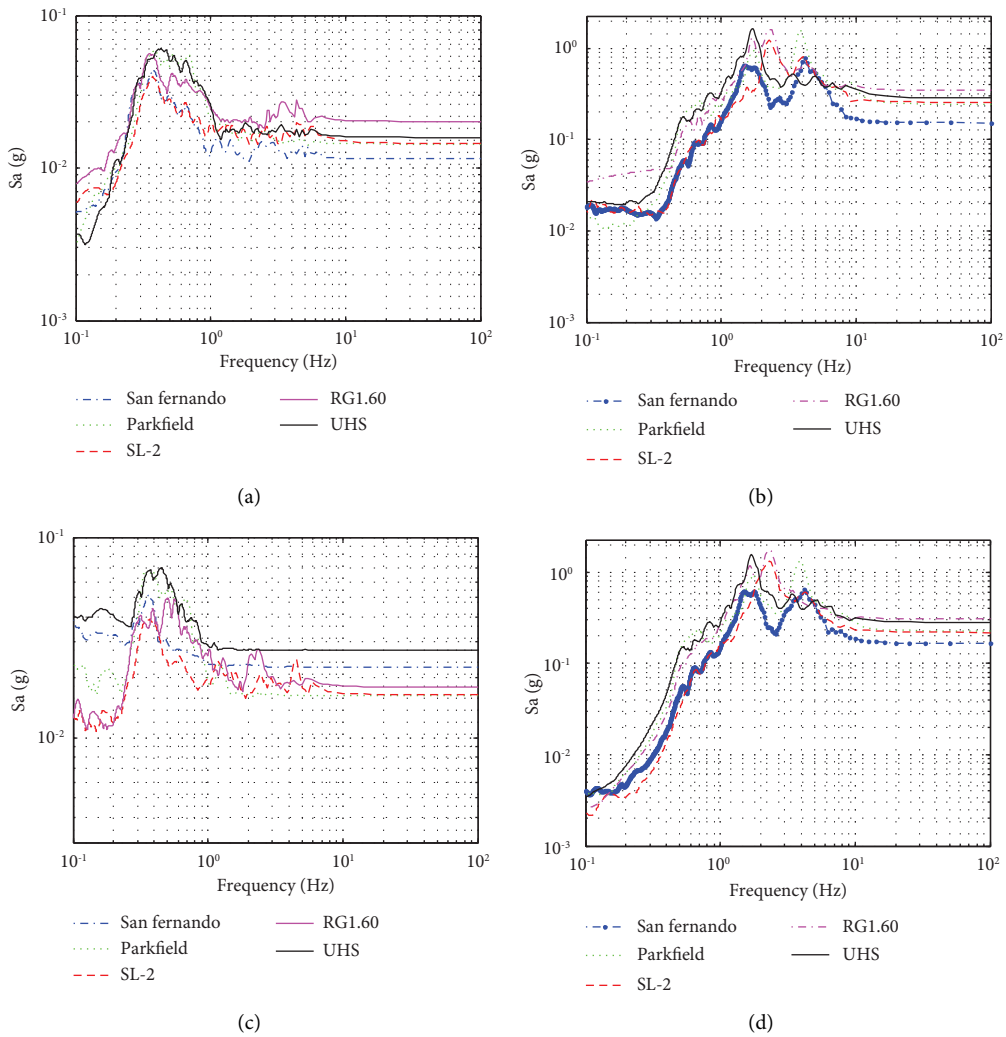

Figure 21: Continued.

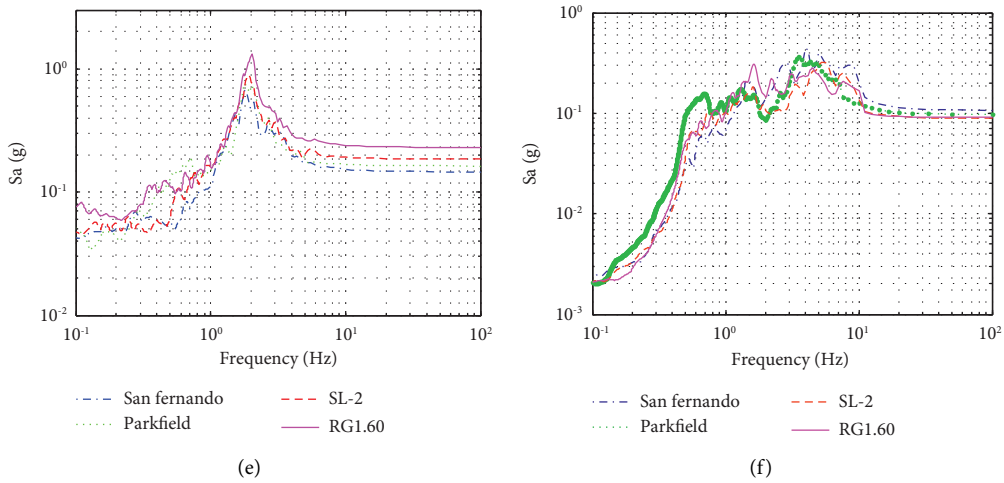

FIGURE 21: Floor response spectrum of the pressure vessel support (A2) (conversion to the prototype). (a) Structure with isolations along the x-direction; (b) structure without isolations along the x-direction; (c) structure with isolations along the y-direction; (d) structure without isolations along the y-direction; (e) structure with isolations along the z-direction; (f) structure without isolations along the z-direction.

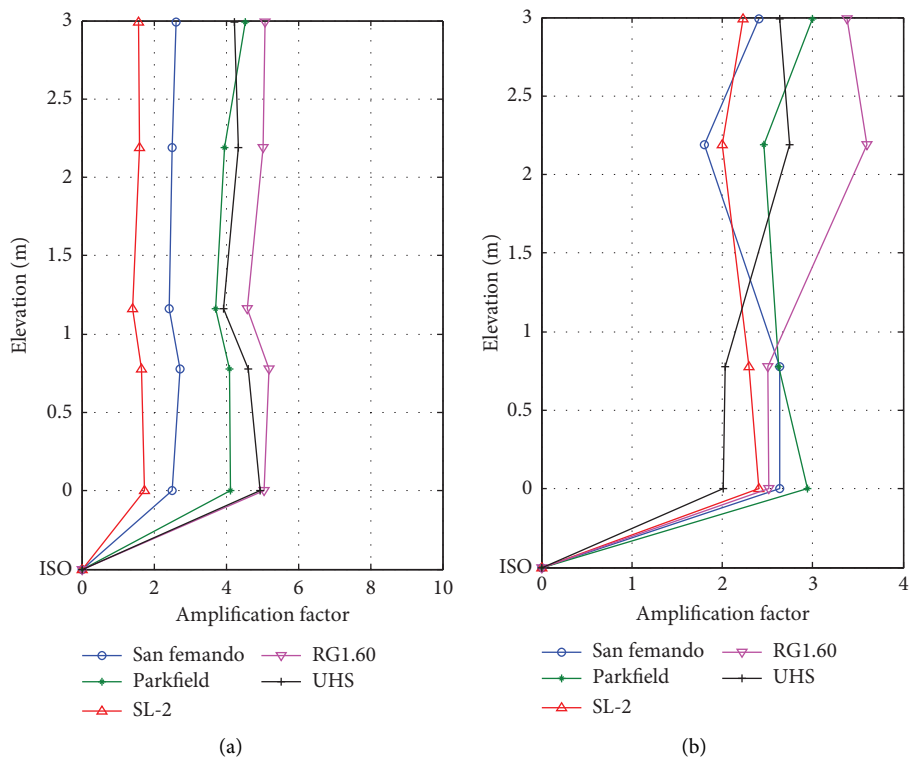

FIGURE 22: Displacement peak under isolation (relative table). (a) Structure with isolations along the x-direction; (b) structure with isolations along the y-direction.

Of the five displacement time histories, the peaks caused by the San Fernando and SL-2 seismic waves were relatively small, namely, slightly greater than 0.5 mm in the isolated state, and the peaks of the other three waves were all greater than 1 mm. In addition, the difference in the peak values of the structure along the x- and y-directions was small. This was mainly due to the large stiffness of the structure itself and the small displacement after the scale reduction of the seismic wave.

The displacement time-history diagram of the isolation bearing was obtained (see Figure 24) by arranging displacement sensors on the shaking table and the base plate. Due to the small similar relation of the dynamic time for the structure and the large compression of the seismic waves, the

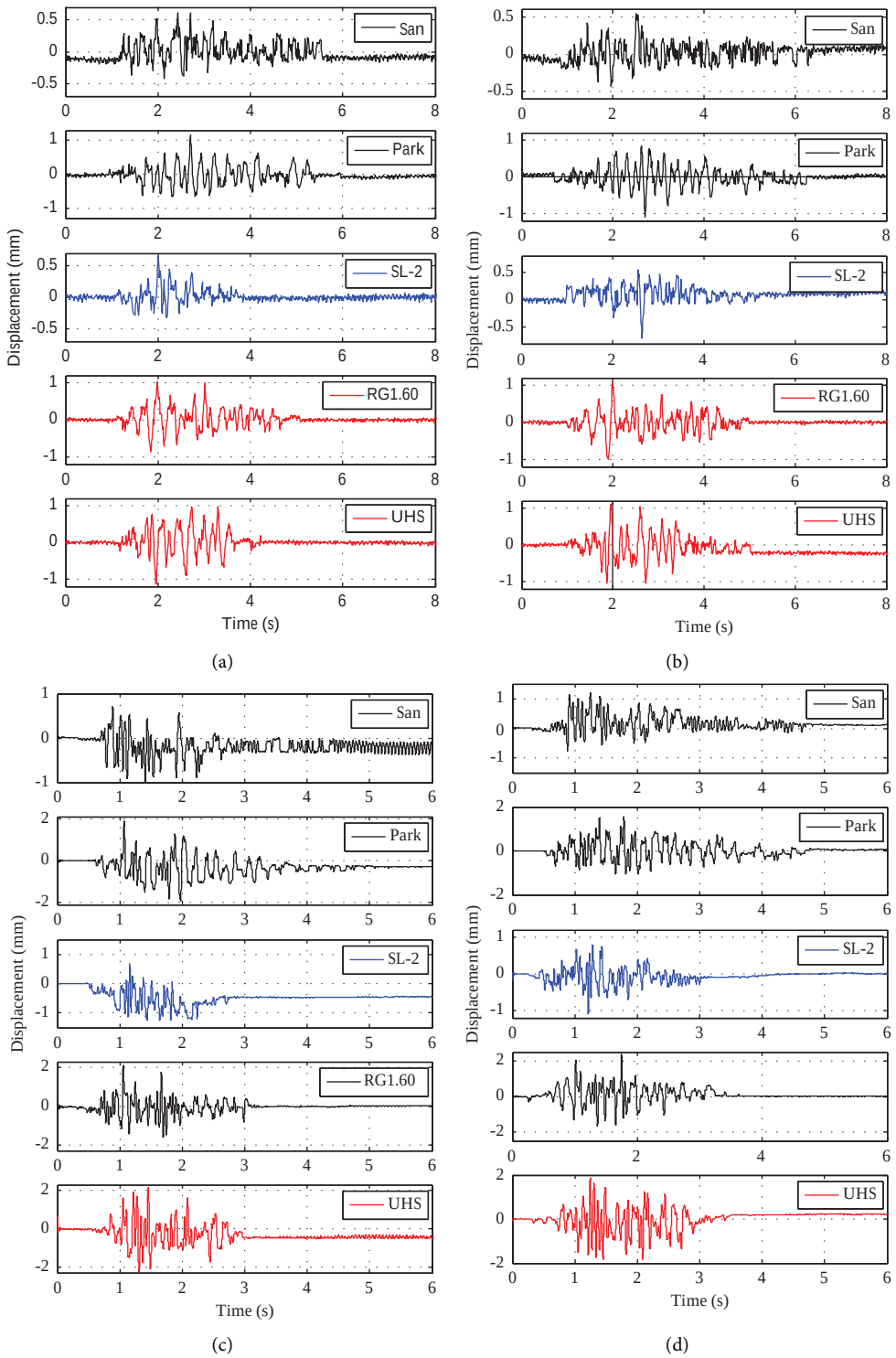

FIGURE 23: Time history of the top reactor plant relative to foundation. (a) Structure with isolations along the x-direction; (b) structure with isolations along the y-direction; (c) structure without isolations along the x-direction; (d) structure without isolations along the y-direction.

displacement time-history range of the seismic waves was small. The displacements of the isolators caused by different seismic waves in the two horizontal directions were different. The maximum relative displacement of the isolators under the action of the artificial wave generated by RG1.60 along the x-direction was 5.04 mm, while that generated by SL-2 was the smallest with a value of 2.07 mm. The maximum relative displacement of the isolators along the y-direction was 2.9 mm under the action of the Parkfield wave, and the minimum displacement peak was 2.14 mm under the action of the SL-2 artificial wave. The design displacement of the isolators was 100 mm, so the displacement of the isolators

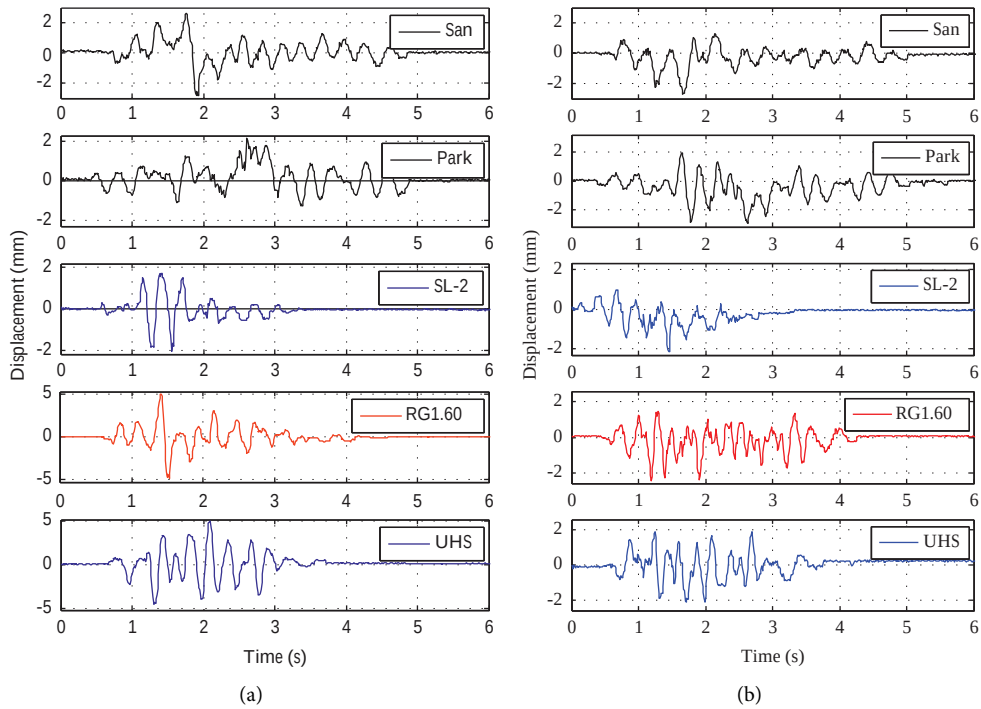

Figure 24: Relative displacement time course of isolated bearing. (a) Along the x-direction; (b) along the y-direction.

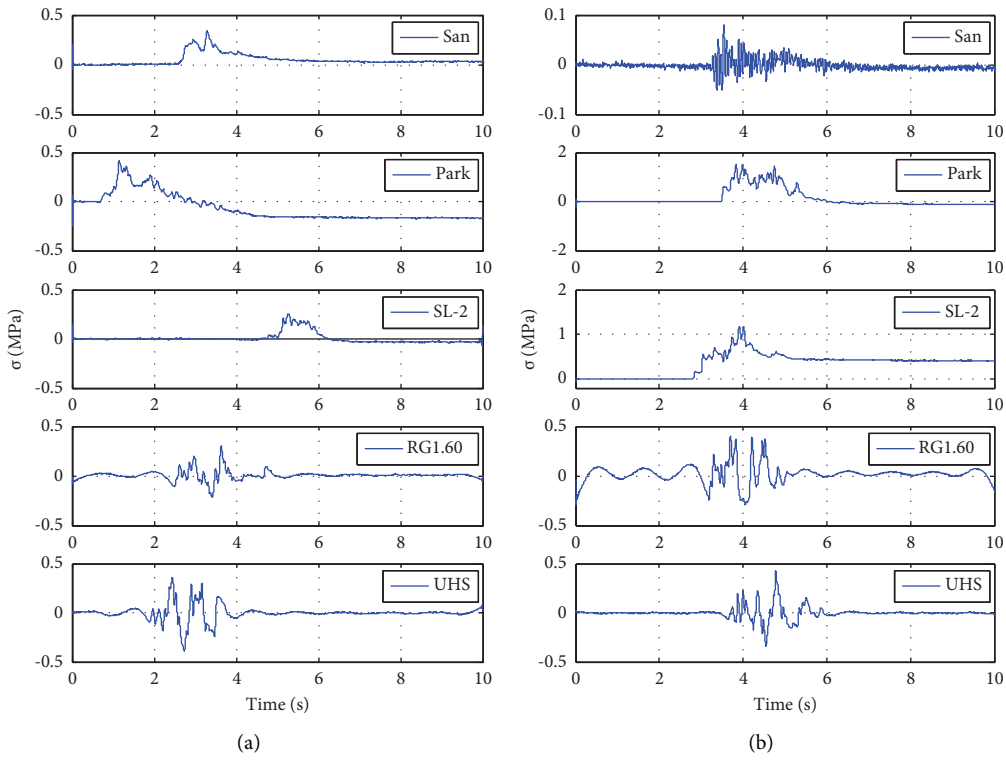

Figure 25: Stress of structure. (a) 0.85 g; (b) 1.28 g.

under a peak acceleration of 0.85 g was far less than the design displacement, and the isolators were in a linear state.

3.4. Stress Analysis. The stress response of the structure was determined through the data processing of the strain gauges arranged in the structure. In the test for the models with seismic isolators, due to the small changes in the strain gauge data of the structure and the great dispersion, only the stress time-history diagrams at the junction of the reactor plant and the spent-fuel plant under the action of 0.85 g and 1.28 g seismic waves in the nonisolated state were investigated, as presented in Figure 25. The stress of the concrete on the outer wall of the structure was small, and it was mainly tensile stress.

4. Conclusions

In this research, a 1/20 scale model of a high-temperature gas-cooled reactor nuclear power plant in China was designed and manufactured, and lead-rubber isolators were designed. Shaking table tests on a scale model with and without isolators were, respectively, carried out, and the dynamic response and the isolation effect of the structure were investigated. The following conclusions can be drawn from the present study:

(1) It was determined from the frequency-domain analysis that different seismic waves had different effects on the dynamic response of the structure and the isolation effect. For different types of ground motion, the isolators effectively reduced the dominate frequency of the structure, exhibited a relatively good isolation effect, and ensured the seismic capacity of the nuclear power plant under "extreme safety" ground motion.

(2) The isolators effectively weakened the peak values of the floor response spectra and reduced the range of the peak value of the frequency. Under the action of different seismic waves, the amplitude of the floor response spectrum corresponding to the artificial earthquake motions generated by UHS was more prominent, which had a greater impact on the seismic resistance of the structures and equipment.

(3) Under the nonisolated state, the amplification factor of structural acceleration under the action of artificial earthquake motions generated by UHS increased notably with the increase in the layer height, and the peak value of the vertex displacement was large. These results indicate that UHS generated based on-site conditions had a great influence on the structure and should be used as the necessary auxiliary verification basis for the seismic calculation of nuclear power plants.

Data Availability

The data used to support the findings of this study are available from the corresponding author on request.

Conflicts of Interest

The authors declare that they have no conflicts of interest.

Acknowledgments

This work was financially supported by the National Natural Science Foundation of China (Grant no. 51978015) and the National Science and Technology Major Project of the Ministry of Science and Technology of China (2018ZX06902016).

References

[1] L. Y. Xu, J. Y. Zhao, and Z. G. Zhou, "Effects of characteristic parameters of isolation system on seismic response of isolated nuclear power plants," *The Structural Design of Tall and Special Buildings*, vol. 29, no. 3, 2020.

[2] D. Cancellara and F. De Angelis, "Nonlinear dynamic analysis for multi-storey RC structures with hybrid base isolation systems in presence of bi-directional ground motions," *Composite Structures*, vol. 154, pp. 464–492, 2016.

[3] M. Kumar, *Seismic Isolation of Nuclear Power Plants Using Elastomeric Bearings*, State University of New York at Buffalo, Buffalo, NY, USA, 2015.

[4] P. Labbe, "Pioneering actual use of seismic isolation for nuclear facilities," in *Proceedings of the 1st Kashiwazaki International Symposium on Seismic Safety of Nuclear Installations*, Kashiwasaki, Japan, November 2010.

[5] A. S. Whittaker, P. Sollogoub, and M. K. Kim, "Seismic isolation of nuclear power plants: past, present and future," *Nuclear Engineering and Design*, vol. 338, pp. 290–299, 2018.

[6] C. C. Yu, C. Bolisetti, J. L. Coleman, B. Kosbab, and A. S. Whittaker, "Using seismic isolation to reduce risk and capital cost of safety-related nuclear structures," *Nuclear Engineering and Design*, vol. 326, pp. 268–284, 2018.

[7] S. S. Parsi, K. M. Lal, B. D. Kosbab, E. D. Ingersoll, K. Shirvan, and A. S. Whittaker, "Seismic isolation: a pathway to standardized advanced nuclear reactors," *Nuclear Engineering and Design*, vol. 387, Article ID 111445, 2022.

[8] Y. Huang, A. S. Whittaker, M. C. Constantinou, and S. Malushte, "Seismic demands on secondary systems in base-isolated nuclear power plants," *Earthquake Engineering & Structural Dynamics*, vol. 36, no. 12, pp. 1741–1761, 2007.

[9] Y. Huang, A. S. Whittaker, and N. Luco, "Seismic performance assessment of base-isolated safety-related nuclear structures," *Earthquake Engineering & Structural Dynamics*, vol. 39, no. 13, pp. 1421–1442, 2010.

[10] Y. Huang, A. S. Whittaker, and N. Luco, "A probabilistic seismic risk assessment procedure for nuclear power plants: (I) Methodology," *Nuclear Engineering and Design*, vol. 241, no. 9, pp. 3996–4003, 2011.

[11] Asce, *Seismic Analysis of Safety-Related Nuclear Structures*, The American Society of Civil Engineers, Reston, VA, USA, 2017.

[12] M. Kumar, A. S. Whittaker, and M. C. Constantinou, "Extreme earthquake response of nuclear power plants isolated using sliding bearings," *Nuclear Engineering and Design*, vol. 316, pp. 9–25, 2017.

[13] M. Kumar, A. S. Whittaker, R. P. Kennedy, J. J. Johnson, and A. Kammerer, "Seismic probabilistic risk assessment for seismically isolated safety-related nuclear facilities," *Nuclear Engineering and Design*, vol. 313, pp. 386–400, 2017.

[14] Asce, *Seismic Design Criteria for Structures, Systems, and Components in Nuclear Facilities*, American Society of Civil Engineers, Reston, VA, USA, 2005.
[15] M. K. Kim and J. H. Kim, "A shaking table test for the evaluation of floor response spectrum of seismic isolated NPP structure," in *Proceedings of the ASME 2016 Pressure Vessels and Piping Conference*, Vancouver, Canada, July 2016.
[16] M. K. Kim, J. H. Kim, and I. K. Choi, "A shaking table test for the evaluation of floor response spectrum of seismic isolated structure," in *Proceedings of the 23 rd Conference on Structural Mechanics in Reactor Technology*, Manchester, UK, August 2015.
[17] D. S. Kim, D. G. Lee, H. C. Cho, and M. B. Park, "A study of the seismic analysis method for interface piping system multi-supported between base-isolated building and non-isolated building," in *Proceedings of the 23 rd Conference on Structural Mechanics in Reactor Technology*, Manchester, UK, August 2015.
[18] D. Hahm and M. K. Kim, "Ultimate failure criteria evaluation of elbow pipe components in seismically isolated NPPs," in *Proceedings of the ASME 2016 Pressure Vessels and Piping Conference*, Vancouver, Canada, July 2016.
[19] X. M. Zhang, L. L. Song, H. J. Chen, S. C. Chen, Z. A. Hu, and Y. Li, "Shaking table test investigation on seismic performance of joint model of immersed tunnel," *Shock and Vibration*, vol. 2022, Article ID 1095986, pp. 1–18, 2022.
[20] X. M. Zhang, W. M. Yan, H. X. He, Y. L. Sun, and S. C. Chen, "Generation of uniform hazard spectrum based on the stochastic method of simulating ground motion and its use in nuclear power plants," *Advances in Civil Engineering*, vol. 2018, pp. 1–12, Article ID 6037863, 2018.
[21] Nrc, *Design Response Spectra for Seismic Design of Nuclear Power Plant*, U.S.N.R. Commission, Norfolk, VA, USA, 2014.
[22] B. Tagliafierro, R. Montuori, and M. G. Castellano, "Shake table testing and numerical modelling of a steel pallet racking structure with a seismic isolation system," *Thin-Walled Structures*, vol. 164, Article ID 107924, 2021.
[23] X. Y. Zhu, G. Lin, R. Pan, and J. B. Li, "Design and analysis of isolation effectiveness for three-dimensional base-seismic isolation of nuclear island building," *Nuclear Engineering and Technology*, vol. 54, no. 1, pp. 374–385, 2022.